Biophysical Journal
Article

Unraveling the mechanism of octenidine and chlorhexidine on membranes: Does electrostatics matter?

Mateusz Rzycki,[1,2,*] Dominik Drabik,[2,3] Kamila Szostak-Paluch,[2,4] Beata Hanus-Lorenz,[2] and Sebastian Kraszewski[2]

[1]Department of Experimental Physics and [2]Department of Biomedical Engineering, Faculty of Fundamental Problems of Technology, Wroclaw University of Science and Technology, Wroclaw, Poland; [3]Laboratory of Cytobiochemistry, Faculty of Biotechnology, University of Wroclaw, Wroclaw, Poland; and [4]Research and Development Center, Regional Specialized Hospital, Wroclaw, Poland

ABSTRACT The increasing problem of antibiotic resistance in bacteria requires the development of new antimicrobial candidates. There are several well-known substances with commercial use, but their molecular mode of action is not fully understood. In this work, we focus on two commonly used antimicrobial agents from the detergent family—octenidine dichloride (OCT) and chlorhexidine digluconate (CHX). Both of them are reported to be agents selectively attacking the cell membrane through interaction inducing membrane disruption by emulsification. They are believed to present electrostatic selectivity toward charged lipids. In this study, we tested this hypothesis and revised previously proposed molecular mechanisms of action. Employing a variety of techniques such as molecular dynamics, ζ potential with dynamic light scattering, vesicle fluctuation spectroscopy, carboxyfluorescein leakage measurement, and fluorescence trimethylammonium-diphenylhexatriene- and diphenylhexatriene-based studies for determination of OCT and CHX membrane location, we performed experimental studies using two model membrane systems—zwitterionic PC and negatively charged PG (18:1/18:1):PC (16:0/18:1) 3:7, respectively. These studies were extended by molecular dynamics simulations performed on a three-component bacterial membrane model system to further test interactions with another negatively charged lipid, cardiolipin. In summary, our study demonstrated that detergent selectivity is far more complicated than supposed simple electrostatic interactions. Although OCT does disrupt the membrane, our results suggest that its primary selectivity was more linked to mechanical properties of the membrane. On the other hand, CHX did not disrupt membranes as a primary activity, nor did it show any sign of electrostatic selectivity toward negatively charged membranes at any stage of interactions, which suggests membrane disruption by influencing more discrete membrane properties.

SIGNIFICANCE The common abuse of antibiotics caused bacteria to develop effective drug resistance over the years. The World Health Organization states that it is one of the biggest threats nowadays. An approach to address this problem is to focus on antiseptic substances that do not have a well-defined molecular target in bacterial cells. As a result, the development of resistance is reduced or even prevented. However, although the substances are commonly used, the knowledge of their mechanism and behavior is limited. Hence, there is a need for more study of these compounds to enable further development. In this work, we employed advanced experimental and computational methods to study the mechanism and selectivity of two commonly used antiseptics, octenidine and chlorhexidine.

INTRODUCTION

The rapidly spreading antibiotic resistance of bacteria has been recognized as a potentially catastrophic threat over the next few years. Because of the common abuse of antibiotics, through genetic adaptation bacteria have developed effective drug resistance (1), and the forecast is not optimistic. The World Health Organization states that it is one of the biggest threats to global health, food security, and development nowadays (2). Millions more people will start dying every year unless new antimicrobial substances are discovered by 2050. This phenomenon is accelerating because of the constant mutations, horizontal gene transfer between the microorganisms, improperly conducted

Submitted January 5, 2021, and accepted for publication June 22, 2021.

*Correspondence: mateusz.rzycki@pwr.edu.pl

Editor: Rumiana Dimova.

https://doi.org/10.1016/j.bpj.2021.06.027

© 2021 Biophysical Society.

This is an open access article under the CC BY-NC-ND license (http://creativecommons.org/licenses/by-nc-nd/4.0/).

antibiotic therapies, and overuse of antibiotics in animal production (3). As a result, substances previously known to save lives will not fulfill their function. A well-known example is the story of penicillin and β-lactam antibiotic resistance (4). One approach to address this problem is to focus on antiseptic substances with a broad spectrum of activity. Such substances do not have a well-defined molecular target in bacterial cells. Interaction with different cellular structures simultaneously makes it harder to develop resistance based on suitable mutations in genetic material. A further advantage is the potential for local application with higher concentration, directly on the skin, mucous membranes, or wounds (5). Another approach is the use of agents with understood and designed molecular selectivity toward the most slowly evolving bacterial structures such as their lipid membrane. Numerous widely used antiseptics belong to the cationic surfactants class. Two of them—chlorhexidine digluconate (CHX) and octenidine dihydrochloride (OCT)—are known for their broad-spectrum activity with a not completely understood molecular mode of action. They are commonly used in various antimicrobial products available on the market, such as Octenisept (Schülke & Mayr, Germany) or Eludril (Pierre Fabre, French), for skin and oral applications (6).

Octenidine dihydrochloride is an antiseptic agent originally described in the 1980s. It is a cationic surfactant that belongs to the bispyridine class (7). Its structure consists of two noninteracting cationic rings separated by a hydrocarbon chain. It exhibits activity against both Gram-positive and Gram-negative bacteria (7,8). A concentration of octenidine less than 1.5 μM (0.94 μg/mL) was reported to decrease the population of tested organisms by more than 99% within 15 min of application (9). It differs from other well-known compounds such as quaternary ammonium compounds because of the lack of an amide and ester component within the structure. As a result, OCT toxicity is lower, and a common quaternary ammonium compound toxic metabolite known as 4-nitroaniline cannot be formed during structural changes (7). OCT is stable over the whole pH range 1.6–12.2, which is particularly important considering varying conditions of healing wounds (10). The wide use of OCT as an antiseptic agent and a number of research articles indicate the incapability of microorganisms to adapt to the presence of this molecule (11). However, the exact mechanism of octenidine action is not well understood. Kodevova et al. noted that OCT creates nontoxic complexes at the site of action (12) It was also indicated that there is strong binding to the negatively charged elements of the yeast cell membrane, leading to disintegration of the cell membrane. When the negatively charged membrane was used as a model and incubated with 3 μM OCT solution, a significant part of it was destroyed after 3 min (12). Selectivity of action was also reported. Recently, a different mode of action was proposed (13). Specifically, because of electrostatic interactions, OCT immediately attaches to the outer membrane, leading to neutralization of the bacterial surface charge. This is followed by OCT hydrocarbon interfering with fatty acyl chains in the outer membrane and inducing strong disorder, disturbing integrity, and causing depolarization and loss of packing order. The literature does not indicate any negative impact of this agent on human epithelial cells or the healing process. Both Brill et al. and Hubner et al. suggested strong adhesion of OCT to bacterial cell membrane components (e.g., cardiolipin) (14,15). It may suggest a selective mechanism of action, as no toxic effect was observed in human epithelial cells. Assadian suggested that the mechanism of OCT is based on interactions with glycerol phosphates present in the microorganism membrane and the enzymatic system, which results in cytoplasmic leakage and cell death (7). Based on available literature, the presumed mode of action is not associated with a specific metabolic pathway or target protein but acts more comprehensively. Most of the currently suggested mechanisms of action involve attack on cell or lipid membrane with electric charge dependency. Also, some works mention the possible occurrence of resistance to OCT (16–18). A significant change in shape, and possible change in membrane composition, was observed to counter the antimicrobial effect of OCT, which may be considered as the first steps in the development of an OCT resistance mechanism. Dopcea et al. reported that OCT exposure resulted in an increased minimal inhibitory concentration (MIC) in *Staphylococcus aureus* and *S. epidermidis* strains (17). In the same study, they reported that the minimal bactericidal concentration, which is the lowest concentration of an antibacterial agent required to kill a bacterium, had increased significantly in a clinical isolate of *S. aureus* (17). In another approach, Shepherd et al. exposed *Pseudomonas aeruginosa* strains to increased concentrations of OCT (18). Their results demonstrate that *P. aeruginosa* can resist great doses of in-use OCT formulations, and furthermore, it can adapt to OCT in a clinical setup, leading to increased OCT tolerance.

The second substance, chlorhexidine, is an antiseptic agent originally described in the 1950s. It is a divalent, cationic biguanidine that exists in three forms: gluconate, acetate, and hydrochloride salt (19). Its net charge is zero, but in solution it dissociates and becomes positively charged. It is most commonly used in concentrations of 0.5–4.0% in the form of gluconate. This compound has a wide spectrum of action against Gram-positive bacteria, but worse (20 times lower MIC value) results are achieved with Gram-negative bacteria (20–22) such as *P. aeruginosa* and *Providencia stuartii*. Some groups report solving this issue by using chelators. The antimicrobial properties of chlorhexidine have remained strong over the years, which suggests limited resistance development by bacteria (23,24). Any observed changes of MIC in the previous century were believed to be caused by composition modification of used model membranes but not increasing

bacteria resistance (23,25). However, Horner et al. draw attention to the increasing number of reports on the reduction in microbial susceptibility to CHX (19). Recently, Copin et al. reported that the spread of community-associated methicillin-resistant *S. aureus* was caused by the acquisition of resistance genes to chlorhexidine agents (26). Also noteworthy are reports collected by Cieplik et al. indicating the presence of CHX resistance at the genetic level in *P. stutzeri* and in different staphylococci (27). The authors also emphasize the need to standardize the concept of resistance in the context of CHX because the research was conducted mainly on Gram-negative bacteria (19). Nevertheless, a few studies investigating the effect of chlorhexidine on Gram-positive bacteria have been conducted. For instance, Cheung et al. concluded that *Bacillus subtilis* is more susceptible to CHX action because more proteins were lost from those cells compared with *Escherichia coli* cells (28). The mechanism of action remains unclear, despite several studies being carried out. Chawner et al. suggested that the mechanism of antimicrobial action of CHX is related to biguanidine structure. In detail, the biguanide group exhibits a strong association with exposed anionic centers on the membrane and negatively charged extracellular matrix's acid phospholipid groups and proteins (29,30). Binding of biguanides to these structures may cause displacement of bivalent Mg^{2+} and Ca^{2+} cations, bound to the cell bilayer, which leads to leakage of potassium cations and protons through the membrane. Therefore, CHX disrupts the osmotic balance of the cell (31). Additionally, CHX hydrophobic regions are not dissolved in the membrane core. As a result, a six-carbon chain linking (coupling) the rings in CHX cannot be incorporated sufficiently in the bilayer. Hence, CHX forms bridges between adjacent phosphate groups of phospholipids and displaces the associated divalent cation from the system (Mg^{2+} and Ca^{2+}). At lower concentrations, CHX causes membrane fluidity reduction and dysfunction both in osmoregulation and in metabolic efficiency of the membrane enzymes, causing leakage of potassium ions and protons from the microbial cell, inhibition of respiratory activity, and transport of dissolved substances (27,32–35). At high concentrations, membrane transition to the liquid crystal phase occurs, which is accompanied by integrity loss and rapid, massive leakage from the cell (29,30,36,37). Another suggestion was proposed by Banerjee et al. in 2013 (38). They examined CHX adsorption on the surface. It was determined that surface charge is one of the most important factors in CHX antimicrobial mechanism of action (38). These findings are consistent with the work by Freitas et al., in which electrostatic effects were emphasized and CHX had a reducing effect on the interfacial tension (39). Costalonga et al. (40) observed noticeable CHX activity in various dental surface models, showing that intrinsic interactions of the drug with the hydrophobic part of the lipid membrane led to disruption of the lipid organization at the interphase. Additionally, the secondary structure of the polypeptide model was changed as a result of CHX action. Moreover, the described interactions between lipid and protein moieties are believed to be present in membranes and may have a specific implication for understanding how antiseptics act on the bacterial membrane (40). Based on the available literature, it can be assumed that the effect of CHX is comprehensive. It not only affects potassium ions, by disrupting osmotic balance, but also interacts with lipid membranes by creating bridges between lipid head molecules.

Despite numerous attempts to unravel the exact molecular mechanism of action for both CHX and OCT, it remains too comprehensive, unspecified, and elusive. However, as mentioned in the Introduction, most of the literature data partially suggest interactions with the membrane by electrostatic selectivity. Based on available knowledge, we have focused on those two aspects. By combining experimental and simulation methods, we attempt to verify the proposed molecular mechanism of action and establish the model action of membrane disintegration based on electrostatic interactions. To enable us to test the electrostatic selectivity hypothesis, we decided to mimic *E. coli* Gram-negative bacteria membrane rich in CL and PG lipids. Specifically, membrane composition was selected based on the negative charge of the outer surface of bacterial cells. Gram-negative bacteria have a negative surface charge because of the presence of phospholipids and lipopolysaccharides (rich in phosphate groups) in the outer membrane (41). We decided to use a model membrane with a highly negative mean ζ potential (-60 mV), which consists of PG (18:1/18:1; DOPG) and PC (16:0/18:1; POPC) in the 3:7 ratio, respectively. As a model of a neutral membrane (with mean surface charge equal to 0 mV), we used pure PC (16:0/18:1; POPC) membrane. In our research, we combined molecular dynamics simulations with various experimental approaches. The experimental models of the membrane were additionally enhanced with numerical simulations on bacteria mimicking membrane (8:1.5:0.5 ratio PE (16:0/16:1 PYPE):PG (16:0/16:1 PYPG):CL (16:0.18:1/16:0.18:1 PVCL2), respectively) (42,43). We studied membrane structure and stability as a function of OCT and CHX concentration by determination of the ζ potential and dynamic light scattering. The localization of the antimicrobial compounds in the lipid membrane was investigated by fluorescence studies with trimethylammonium-diphenylhexatriene (TMA-DPH) and DPH probes. These probes react to changes occurring in the inner part of the bilayer at the level of hydrophobic tails and hydrophilic heads. This allowed us to determine the preferential location of accumulation of the compounds in the lipid membrane. Mechanical changes, specifically bending rigidity, as a function of OCT and CHX concentration were measured using flicker-noise spectroscopy. Finally, we investigated the leakage of carboxyfluorescein (CXF) encapsulated in the liposomes to identify the potency of membrane-disrupting antibacterial

activity and selectivity of compounds. All these various aspects were verified using molecular dynamics simulations, which allowed the analysis of the system at the atomic level, as well as enabling us to overcome the limitations of the experiments. The main aim of our research was to verify the prevailing opinion that the interaction and antiseptic effect of OCT and CHX result from the electrostatic interactions of the molecules with negatively charged elements on the outer surface of bacterial cells. In our study, we managed to experimentally test the hypothesis of the electrostatic selectivity of two investigated agents, OCT and CHX. Through the use of molecular dynamics simulations, we were able to independently verify this hypothesis and to propose alternative mode of action.

MATERIALS AND METHODS

Materials

POPC and DOPG lipid powders were purchased from Avanti Polar Lipids (Alabaster, AL). Fluorescent dye Atto 488 DOPE was purchased from ATTO-TECH (Siegen, Germany), and both TMA-DPH and DPH were purchased from Sigma-Aldrich (Darmstadt, Germany). Octenidine dihydrochloride was purchased from Ferak (Berlin, Germany). Digluconian chlorhexidine was purchased from MP Biomedicals (Eschwege, Germany). CXF was purchased from Merck (Kenilworth, NJ).

Large unilamellar vesicle preparation procedure

The large unilamellar vesicles were formed using the extrusion method. Lipids were dissolved in chloroform and dried under a stream of argon, followed by 12-h vacuum treatment to ensure complete organic solvent removal. The resulting dry lipid film was hydrated with an aqueous solution and vortexed to obtain a milky suspension. The obtained mixture was extruded through polycarbonate filters with 100-nm pores (Whatman, Dassel, Germany). The quality of the liposomes was tested using the dynamic light scattering technique (Zetasizer Nano ZS; Malvern, Malvern, UK).

Giant unilamellar vesicles preparation procedure: electroformation

The modified method of model membrane formation for giant unilamellar vesicles (GUVs) was used. Briefly, 10 μL of 1 mM POPC and fluorescent probe mixture (1 m%) in chloroform was distributed equally along the platinum electrodes and dried under reduced pressure for 1 h. The electrodes were then submerged in aqueous nonconductive solution, and a square 1-Hz AC electric field was applied for 2 h with increasing voltage up to 4 V in a custom polytetrafluoroethylene electroformation chamber (44).

Vesicle fluctuation spectroscopy

Thermally induced shape fluctuations of GUVs can be used to determine the mechanical properties (bending rigidity). The series of images of GUVs were recorded using fluorescence confocal microscopy. A Stellaris confocal microscope (Leica, Wetzlar, Germany) was equipped with an HC PL APO 86×/1.20 water immersion objective (Leica). 256 × 256 pixel images were recorded with a hybrid (HyD; Leica) detector with pixel size ranging from 0.088 to 0.136 μm with video integration time ranging from 130 ms up to 190 ms depending on the zoom magnitude. Samples were illuminated with white laser set at 488 nm; emitted light was recorded from 500 up to 600 nm. The series usually consisted of 1200 images. The two-dimensional liposome images are transformed to the three-dimensional Helfrich model using both the average-based and statistical approaches. Then, the radial position of the bilayer, extracted from images, is used to construct angular autocorrelation curves. In the average-based approach, autocorrelation curves are decomposed into Legendre polynomial series and are plotted as a function of fluctuation mode so the bending rigidity coefficient can be determined. In the statistical approach, autocorrelation curves are decomposed into Fourier series, and a frequency histogram of amplitudes for each mode of fluctuation is calculated. The histogram is then used for determination of the bending rigidity coefficient as described in detail elsewhere (45). The radii of investigated vesicles ranged from 3.3 up to 12.8 μm. Selected videos of vesicles treated with investigated agents are presented in the Supporting material (Videos S1 and S2, POPC and POPC/DOPG vesicles; Videos S3 and S4, POPC and POPC/DOPG vesicles treated with 0.1 OCT/LIP.; Videos S5 and S6, POPC and POPC/DOPG vesicles with 0.1 CHX/LIP.).

ζ-potential determination and dynamic light scattering

ζ-potential and dynamic light scattering measurements were performed on 1 mM liposomes. Measurements were performed in 10 mM NaCl solution. Liposomes were titrated with 1.5 mM octenidine solution in the same buffer. Measurements were performed using Zetasizer Nano ZS (Malvern). Each sample was left for 15 min after adding a solution of octenidine to obtain equilibrium in the sample. ζ-potential measurements were used for partitioning coefficient determination using the established approach (46). However, this approach can only be applied if a net charge of the particle and the proportion and effective charge of the ionic phospholipids in the vesicles are known and are not equal to 0. All performed experiments were repeated three times unless specified differently in the particular Materials and methods section.

CXF leakage measurement and sample preparation

Encapsulation of CXF

60 mM pure POPC or a 3:7 ratio of DOPG/POPC liposomes, respectively, with 50 mM CXF in buffer (100 mM KCl, 10 mM Tris, 10 mM MES (2-(N-morpholino)ethanesulfonic acid) (pH 7.0)) were prepared. Solutions were extruded by 100-nm filters (Whatman, Dassel, Germany). The polydispersity of the population was checked and did not exceed 10%. Liposomes were purified by the dialysis method, based on Micro Float-A-Lyzer dialysis membranes (Sigma-Aldrich) with the threshold ∼50 kDa. Lipid concentration was determined using ammonium ferrothiocyanate colorimetric method to assess the loss after ultrafiltration. The final lipid concentration was equal to 20 mM. Kinetics of release of CXF was measured with a Horiba Fluoromax 4 spectrofluorometer (λ_{ex} 492 nm, slit, 1 nm; λ_{em} 517 nm, slit, 1 nm; Horiba, Piscataway, NJ) for ∼700 s with a time step of 1 s. 4 μL of liposome solution was added to 3 mL buffer in measuring cuvette. This corresponds to 27 μM final lipid concentration during the measurement.

Kinetics of CXF leakage

Kinetics lasted for 700 s with a time step of 1 s. For each measurement, the intensity of the reference detector was recorded to include light source fluctuation corrections. This correction has already been applied in the results below. The solution was injected with a Hamilton syringe to the bottom. A magnetic stirrer was present in the measuring cuvette to enable equal distribution of agents. After ∼100 s of signal recording, octenidine or chlorhexidine solution was added to obtain the appropriate ratio of tested particles and lipids. After 500 s of signal recording, 15 μL of 5% solution

of Triton-X100 was added (as a positive control), leading to complete micellization of the membrane and release of all CXF into the solution.

Localization study using TMA-DPH and DPH fluorescent probes

To investigate the incorporation of agents into membranes, the DPH and TMA-DPH fluorescence probes were selected. Liposomes were prepared with a probe concentration of 0.5 mol%. The concentration of all investigated lipid vesicles was equal to 1 mM in 10 mM NaCl solution. Either OCT or CHX was added to the liposomes and followed with incubation for 1 h to obtain equilibration. The measurement was made using the SpectroFluoromax 4 spectrofluorometer (Horiba). The excitation wave λex was equal to 350 nm, and emission was in the range of λem 360–520 nm. Both slits were 2 nm wide.

Quantum mechanics

Quantum level calculations were performed using the Gaussian 2016 software package (47). The equilibrium geometry of OCT and CHX molecules was calculated at the HF/6–311+g level of theory. The solvent effect was taken into consideration using the integral equation formalism of the polarizable continuum model IEFPCM. Supplementary analysis based on the construction of the Hessian matrix (the matrix of second derivatives of the energy with respect to geometry) was also performed for further use in the force field parameterization for further molecular dynamics (MD) study. The specific geometric and electronic data such as bond lengths, angles, dihedrals, and charge distribution were extracted from a Hessian matrix. Those parameters are crucial for the construction of the force field used in MD simulations, as described below. The charge distribution was determined from the RESP charge calculations as being the most adapted to reproduce the molecular behavior with the subsequently used CHARMM force field. For logP determination, the octanol/water partitioning coefficient was calculated using SCIGRESS software (SCIGRESS, Molecular modeling software, FQS Poland, ver. FJ-3.3.3).

MD simulations

Several MD systems were constructed for studying the antiseptic agent and lipid membrane interactions and behavior. Three types of membrane systems were assembled in CHARMM-GUI (48) and investigated afterward: neutral (NLM), pure PC (16:0/18:1; POPC); negatively charged (NegM), 3:7 PG (18:1/18:1; DOPG):PC (16:0/18:1; POPC) lipid ratio, respectively; and bacteria mimicking (BacM), 8:1.5:0.5 PE (16:0/16:1; PYPE):PG (16:0/16:1; PYPG):CL (16:0.18:1/16:0.18:1; PVCL2) lipid ratio, respectively. Two different concentrations of antiseptic agents (OCT and CHX) were investigated: lower 1:80 agent/lipid (80 lipid system) and higher 1:26 agent/lipid (182 lipid system). A snapshot of the system's initial state is presented in Figs. S1 and S2. The lipid bilayers were solvated with 400 mM NaCl solution including 100 water molecules per lipid. Such a high ion concentration was selected given the fact that both substances, OCT and CHX, are antimicrobial agents and are often used on open wounds (blood) or in the mouth (saliva). Both blood and saliva are known for their buffering properties. Salt is present in much higher concentrations in the blood than in our simulations, and yet an antimicrobial effect is still present. Additionally, we performed simulations without additional ions to evaluate their impact on agent behavior. The TIP3P water model was employed. Finally, self-assembly of lipid systems was investigated. Systems with pure PC (16:0/18:1 POPC) lipid molecules (180 lipid particles) randomly distributed in space with or without the presence of an additional agent (240 OCT or CHX particles) were created. After brief minimization, they were hydrated as previously described.

MD simulations were performed using the GROMACS (version 2018.3) package with the CHARMM36 force field. Every system was first minimized using the steepest descent algorithm for energy minimization. Calculations were carried out in the NPT ensemble (constant number of particles, pressure and temperature) using a Berendsen thermostat and barostat including semi-isotropic coupling at $T = 303.15$ K and $p = 1$ bar. The initial part of the NPT calculations was performed using the leap-frog integrator with a 1-fs time step. Subsequently, for the further NPT ensemble at $T = 303.15$ K and $p = 1$ bar, a Nosé-Hoover thermostat and Parrinello-Rahman barostat were applied. The second part of long-run production was carried out for at least 400 ns using the leap-frog integrator. Chemical bonds between hydrogen and heavy atoms were constrained to their equilibrium values using the LINCS algorithm, and long-range electrostatic forces were evaluated using the particle mesh Ewald method, which allowed us to employ an integration time step of 2 fs. Based on simulated pure membranes, the action of antiseptic agents was investigated. Molecules were placed on average 2 nm above the membrane leaflet. The same procedure was employed for constructed lipid/agent systems. For visualization and analysis purpose we used GROMACS tools, Visual Molecular Dynamics (49), and Diffusion Coefficient Tool (50). Selected videos of numerical bilayers treated with investigated agents are presented in the Supporting material (Videos S7 and S8, NLM and BacM with OCT; Videos S9 and S10, NLM and NegM with CHX).

Statistics and data representation

To test for the significant difference between the parameters, the one-way analysis of variance test was used with the significance level at 0.05. The Tukey test was used as a post hoc test. All statistical analysis was performed using the OriginPro 2015 (OriginLabs) software. Average values are presented with standard deviation.

RESULTS AND DISCUSSION

OCT

Location and behavior

The general behavior of the OCT-membrane interaction was first assessed using MD. In control NLM, the OCT particle (Fig. 1 *A*) reached the surface and anchored after 140 ns. In BacM membrane (mimicking the bacterial one), the OCT particle reached the surface faster, which was followed by anchoring after 45 ns. The entire particle incorporation to the negative membrane (NegM) lasted the longest—220 ns. However, one acyl chain anchored after 120 ns, leaving the second one and the spacer above, and it took almost 100 ns more for the second one to attach. After incorporation in the membrane, OCT took the shape of a staple, penetrating the monolayer with two acyl chain ends (as shown in Fig. 1 *B*).

Clearly, the OCT interaction was strongest with the BacM, as both reaching the surface and anchoring were faster. Movement of incorporated particles in the lateral plane of the membrane was observed after incorporation in both membranes. Furthermore, in all simulated model membranes, OCT particle penetrated the membrane deeply inside, anchoring at the carbonyl-glycerol region. It is noteworthy that on the BacM, the hydrogen atoms from the agent's acyl chain statistically penetrated the deepest,

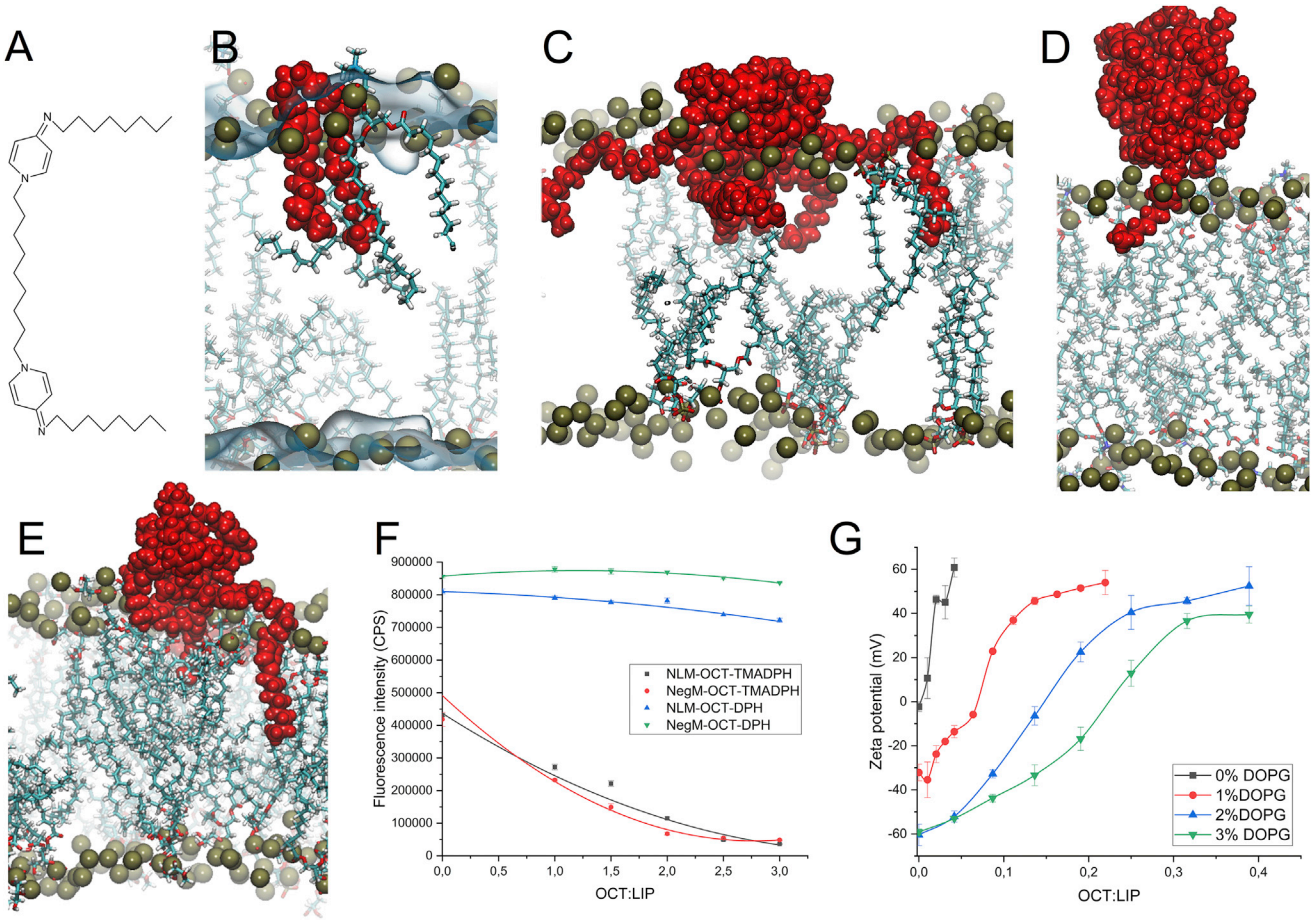

FIGURE 1 (*A*) Chemical structure of OCT, (*B*) single OCT molecule incorporated into BacM, (*C*) visualization of spread aggregate of OCT on BacM membrane, (*D*) visualization of balloon-shaped OCT aggregate on NLM, and (*E*) visualization of spread aggregate of OCT on NegM membrane; in all snapshots, several lipids have been hidden for clarity. OCT molecules, phosphorus atoms from lipid headgroups, and water surface have been colored in red, olive, and blue, respectively. (*F*) Fluorograms from DPH and TMA-DPH probes indicating OCT localization in carbonyl-glycerol region and (*G*) ζ-potential changes due to OCT titration for the POPC membranes with various DOPG composition. To see this figure in color, go online.

reaching 8.7 ± 2.9 Å level from bilayer center. In the case of the NLM and NegM, the OCT reached the 9.8 ± 2.9 and 9.9 ± 2.8 Å levels, respectively, from the bilayer center. Only the NLM and NegM pair was not statistically distinct. The detailed location of system components such as lipid fragments or agent molecules has been presented in the partial density charts in Figs. S3 and S4. The OCT particle directed its acyl chains toward the membrane, leaving the spacer above (as shown in Fig. 1 *B*). It could possibly be due to the distribution of the OCT positive charges on acyl chains. Almost all types of lipid membranes exposed to OCT action showed slight differences in thickness and area per lipid (APL) (see Table S1). A noticeable decrease after OCT incorporation was observed in the majority of cases. Only in the case of the PG lipid and the NegM system was an increase observed. Furthermore, the incorporation process did not differ between the NegM and NLM; hence, interaction between the positive chains and negatively charged heads of lipids could not be considered as a factor influencing incorporation into the membrane when a single OCT molecule was simulated in the system. Similar OCT behavior was observed in systems without NaCl ions. OCT is anchored to the bilayer in a staple shape in all systems. Interestingly, the staple shape was more extensive compared to 400 mM NaCl systems and the process of incorporation was much faster—35, 20, and 120 ns in the NLM, BacM, and NegM, respectively. This was also followed by a significant increase of OCT's APL values compared with systems with ions (see Table S2). Similar incorporation was observed by Kholina et al. in PE-PG membranes (51).

Afterward, the simulations with an increased number of OCT particles were investigated to study aggregation behavior. A stable aggregate was formed at the initial phase of each of the systems. After several nanoseconds, it interacted with the membrane. Snapshots are presented in Fig. 1, *C–E*. In all of the investigated membrane systems, OCT interaction with the lipid headgroups could be

observed over ∼300 ns. On the NLM, the aggregate anchored inside the membrane purely by one tail, forming a balloon shape that does not interact with lipids. OCTs on the BacM behave differently; the aggregate settled down and spread on the membrane surface, penetrating it heavily with acyl tails. A hybrid model appeared in the NegM system, in which at the initial state OCT particles gathered together, forming a balloon-shaped aggregate similar to that in the NLM system. It settled down on the membrane surface and anchored inside the bilayer by two tails afterward. The NegM exhibits comparable behavior to the NLM, although the first molecule interaction with membrane was clearly faster. To this end, we focused on the incorporation of OCT into membrane systems. The provided phenomenon can be seen by comparing the thickness parameter, which illustrates the growth of lipid surface area in the BacM with greater agent concentration because of higher surfactant penetration (see Table S1). It is noteworthy that it is directly related to the change in the value of the area per molecule (APM) because of the incorporation of OCT aggregate. This indicates the level of interaction between the OCT aggregate and the lipid bilayer. The occupied OCT area in the BacM is equal to 50.1 ± 3.2 $Å^2$ and is almost twice as large as in the NLM, where it is 27.5 ± 6.1 $Å^2$. Additionally, the changes of APL, APM, and thickness for all model systems are presented in Table S1. Slightly different OCT dynamics were observed in the 0 mM NaCl NLM system. In this case, the agent formed a balloon-shaped aggregate; however, it did not incorporate into the bilayer. It stayed in the water phase, slipping on the membrane surface (see Fig. S7). The OCT aggregate completely ignored the membrane. Interestingly, when a system with one anchored OCT in the membrane was employed, the rest of the OCT particles partially followed that manner and incorporated into the membrane (see Fig. S8). This suggests that high salt concentration in solvent prevents OCT from self-aggregation and significantly increases the affinity toward membranes. On both the BacM and NegM, we did not observe substantial permutations such as in the NLM. OCT particles gathered and settled down on the membrane surface, penetrating it with a couple of acyl chains. Similar to before, on the BacM OCT aggregate was more spread and flattened, whereas on the NegM it was more soaring, in the shape of a balloon with a couple of chains anchored. Here, we also noticed a reduction trend in APM, especially in the NegM and BacM systems (see Table S2). Additionally, the lateral diffusion was calculated to check the possibility of OCT preferential interaction with a lipid type, as presented by Kholina et al. (51). In this hypothesis, the radial distribution and diffusion coefficient were used to estimate the level of the propensity for interaction with antiseptics. Our results did not show any strong affinity toward any type of lipid molecule (see Table S3). Our results revealed also that the presence of the agent directly affects the diffusion of all lipids in the system. This is similar to Kholina et al.'s conclusions (51).

We used DPH and TMA-DPH fluorescence probes to experimentally confirm the location of OCT molecules in membranes obtained from MD studies. The location of OCTs in the membrane after incorporation is in the hydrophobic core, close to the heads of hydrophilic lipid membranes. Both of the selected probes are known to be strongly affected by the influence of environment polarity on fluorescent intensity. Therefore, the intensity of their quantum fluorescence in water is significantly lower compared to after localizing in the hydrophobic part of the membrane (52,53). Both probes are also sensitive to the spatial ordering of lipids. Specifically, the DPH probe's fluorescence is known to be a function of the acyl-chain region of the lipid membrane (54), whereas its modification, TMA-DPH, allows for determination of the carbonyl-glycerol region (54–56). Fig. 1 *F* illustrates fluorescence intensity changes at peak value for both probes as a function of the OCT/Lipid ratio for both the NLM and NegM. In both membranes, significant changes were observed for the TMA-DPH probe, whereas no major changes were observed in the case of the DPH probe. Detailed fluorograms for both probes are presented in Fig. S13. Such results suggest an accumulation of the OCT molecules in carbonyl-glycerol, which corresponds perfectly with our results from MD, in which preferential surfactant localization took place in the upper layers of the membrane. Such results could initially suggest a lack of disturbances in the alkyl-chain region. Poojari et al. (57) showed that DPH may not directly reflect information about acyl-chain region packing when additional molecules other than lipids are present. This is especially crucial when the molecule is large and amphipathic (like OCT). Furthermore, as suggested by Nazari et al. (58), the detergent molecules mix poorly with the lipid ones, resulting in segregation into detergent-rich clusters that disrupt the membrane locally, whereas the rest of the membrane with the majority of DPH is only a little affected. Malanovic et al. (13) showed by x-ray scattering on model membranes with PE that disruption in the hydrophobic region was observed. It is possible that OCT particles localized in the carbonyl-glycerol region are inducing acyl-chain packing changes that do not influence the DPH probe behavior. To this end, we performed analysis of order parameter on MD systems (see Fig. S11) containing PC and PE. We showed that differences in order parameter after OCT incorporation into the membrane were observed for PE lipids, but not for PC lipids, in the model membrane systems investigated here. Therefore, we may conclude that there is a high possibility of no direct interaction at the hydrophobic core level of the bilayer and preferential accumulation occurs in the membrane surface area in NegM and NLM membrane systems. In the case of the BacM system, an indirect influence of OCT on the

acyl-chain region was observed that is supported by the experimental results of Malanovic et al. (13).

ζ-potential measurements and partition coefficient

Subsequently, we decided to study membrane structure and stability in function of OCT concentration by determination of the ζ potential and dynamic light scattering and to evaluate the influence of membrane charge on interaction strength as well. The results presented in Fig. 1 *G* indicate a different, less rapid nature of the interaction between OCT and the NegM compared with the NLM. Specifically, the slope of the ζ-potential change was highest for the neutral membrane (16 mV/m%) and slowly decreased with an increase of DOPG in the membrane (7.5, 6.2, and 6.0 mV/m%, respectively). The average size of vesicles determined using dynamic light scattering remained unchanged (see Fig. S15). The ζ-potential changes are not correlated with pH, which remains steady in various agent concentrations (see Fig. S17).

The lipid/water partition coefficient determined from ζ-potential measurement (Fig. S18) was equal to 2.3 ± 0.2 in charged membrane (1, 2, and 3% DOPG) systems (46). Interestingly, this value is significantly smaller than the obtained logP value using the SCIGRESS calculation tool, where it was equal to 9.25. Such a difference highlights the complicated nature of interaction between the OCT and the membrane. Because membranes are much more complex structures than the octanol used in logP determination, the difference between the partition coefficients is not surprising. The magnitude of the difference can lead to the conclusion that interactions between OCT molecules are stronger than between OCT and membrane. This is also in agreement with MD simulations and literature data (59), as it has been reported that OCT tends to form aggregates in water. Nonetheless, OCT directly affects the liposome surface charge, leading to its continuous growth, suggesting that more OCT is located in the membrane than in water. However, that does not necessarily need to be the correct conclusion, because the ζ potential is located above the membrane and OCT particles tend to form aggregates above the membrane surface. The initial electrostatic effect could push OCT particles in the vicinity of the membrane, although particles tend to form aggregates on the membrane surface rather than incorporate into the membrane. This view is additionally supported when the evolution of ζ potential is taken into account in low concentrations of the antimicrobial agent. In the case of the NLM, the difference between 0 and 0.03 of OCT/LIP equals 63 mV, but with increasing DOPG content it decreases to 19, 8, and 6 mV, respectively. The initial conclusion suggests that the more negatively charged the membrane is, the lower the ability of OCT to incorporate into the membrane. However, it is also possible that aggregation is stronger on the negatively charged surface of the membrane, which increases its graininess. As a result, vesicle topology is changed by incorporated anchors, increasing its roughness and friction and hence influencing the outcome of ζ measurement. Moreover, we assume that OCT forms aggregates preferentially to minimize the entropy of the system. Because the ζ potential is located above the membrane interphase, it is possible that, as stated previously, the less rapid character of ζ-potential change means equal or more OCT on the membrane (but not necessarily in the membrane). It also could suggest a very sophisticated antiseptic mechanism of selectivity that is based on how the particle is incorporated into the membrane. This could be related to interaction with negatively charged lipid headgroups but also to membrane curvature and/or other macroscopic properties. Interestingly, results from TMA-DPH and DPH suggest that more rapid increase of ζ potential in the NLMs is not due to OCT incorporation, as for both the NegM and NLM, the incorporation in carbonyl-glycerol is not significantly different. This strengthens the conclusion that an increase in ζ potential for membranes, especially the NegM, is related to the formation of balloon aggregates rather than the rapid incorporation into the membrane of OCT in the first place—especially because, regardless of the charge and the amount of delivered OCT, we observe continuous linear changes in the probe's environment, which results in a decrease in fluorescence intensity.

Destructive effect of agent and selectivity

Finally, we examined the effect of OCT on membranes in terms of disruption of self-assembly. The idea of this simulation is to investigate inverse emulsification of the lipid molecules suspended randomly in water (see Fig. S12). We performed membrane self-assembly studies in the presence of OCT particles. Provided that OCT is not interacting with the membrane, the lipids should self-assemble without any problems. In the case of randomly distributed PC lipids without OCT, formation of a bilayer was observed after 60 ns with a 580 kcal/mol increase in van der Waal (VdW) energy from the initial system to the self-assembled one. Unlike the potential energy, VdW component does not decrease over time when aggregation of components that constitute a significant volume of the simulated particles system occurs. It is expected that aggregation will induce local crowding of particles. In the case of crowding, the VdW energy component will increase to a certain value, higher than the initial one. One can conclude that the electrostatic energy component, being much more negative than at the beginning of the simulation and lowering importantly over time, is the driving force of observed aggregation phenomenon. The entropic changes in MD systems are taken into account indirectly, which could be concluded as the electrostatic driving force. However, in reality, it may have its origins in hydrophobic forces driving the self-assembly of molecules even at the cost of a higher VdW energy component. During the simulation, because of the hydrophobic effect, lipids formed a bilayer, which is

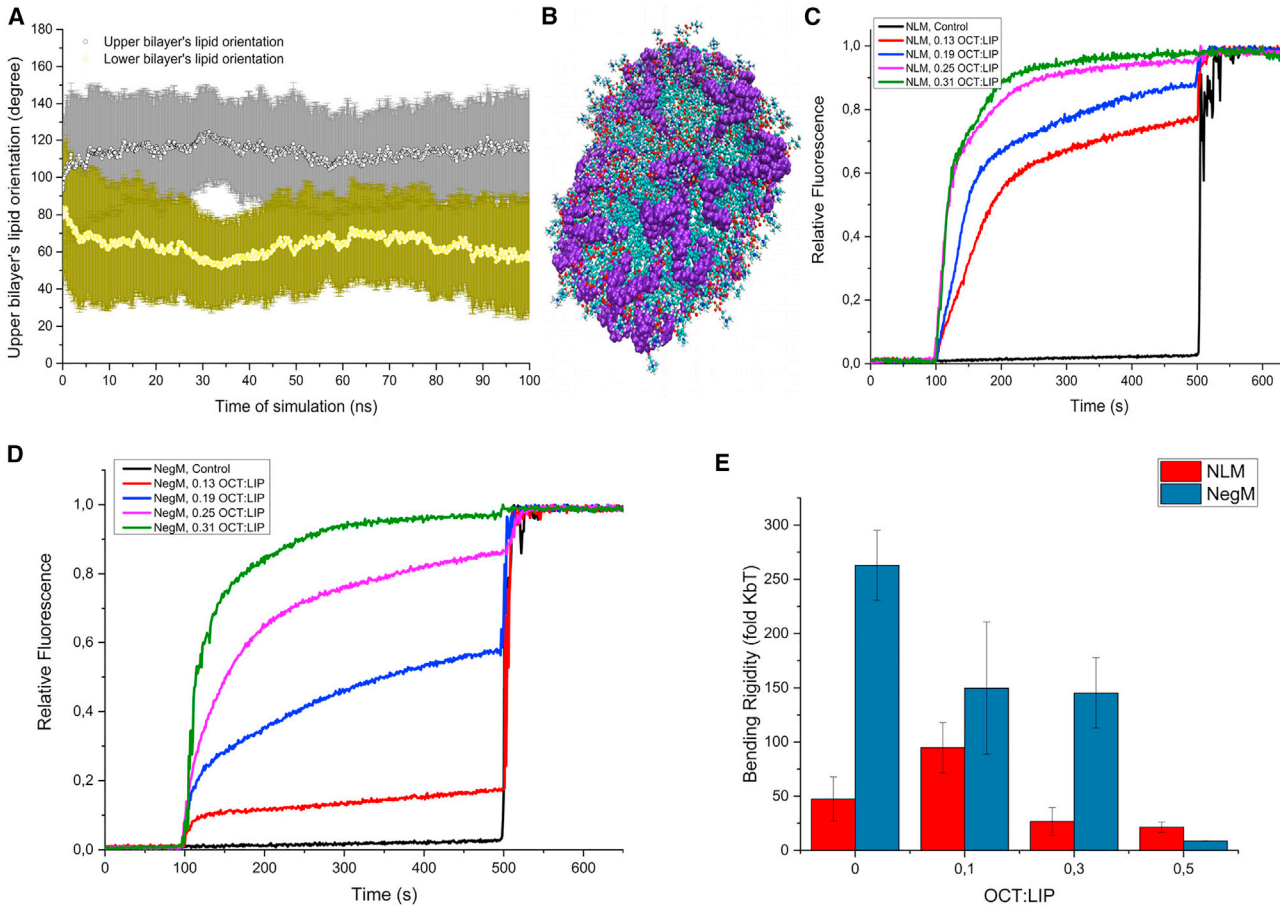

FIGURE 2 (*A*) Self-assembly MD simulation presenting individual lipid particles orientation during disrupted membrane formation by OCT particles, (*B*) visualization of doughnut-like membrane structure after self-assembly accompanied by OCT particles, (*C*) CXF leakage from NLM after OCT addition at 100 s, (*D*) CXF leakage from NegM after OCT addition at 100 s, and (*E*) bending rigidity analysis introduced by statistical approach; results obtained from vesicle fluctuation spectroscopy. To see this figure in color, go online.

associated with the displacement of a significant amount of water molecules from the core interior. However, in the case of the system with OCT molecules, formation of a bilayer did not occur. Evolution of the system is presented in Fig. 2 *A*. Instead, a doughnut-like structure covered with OCT was formed, which is presented in Fig. 2 *B*. The VdW energy increase equaled 435 kcal/mol. This suggests that OCT, as an agent influencing the self-assembly process of the membrane, has a significant impact on its structure and/or fluidity.

Furthermore, the destructive effect of the membrane was investigated experimentally by observing the leakage of CXF loaded inside the liposomes. CXF is a probe that has a self-quenching effect in high concentration; therefore, its fluorescence decreases with increasing concentration (60,61). This makes it commonly used as a tracer agent. Both the NLM and NegM systems were measured. The change in relative fluorescence is presented in Fig. 2, *C* and *D*. Increased volumes of OCT were added to the successive measurements, maintaining the same concentration of liposomes to study the effect of higher surfactant dose on liposome damage. Based on the obtained results, there was a noticeable tendency: the higher the dose of the OCT, the higher the quantity of CXF released from the liposomes. Doubling the initial dose 0.13 OCT/LIP resulted in a doubling of acceleration of the leakage. The quickest leakage observed for the 0.31 OCT/LIP ratio occurred after ~180 s. In the case of the NegM, the results are more varied. As before, raising the dose resulted in a faster reaction, but here the original 0.13 OCT/LIP dose caused a small leakage of CXF. Doubling the dose allowed us to observe much stronger fluorescence and lipid damage within ~200 s from the start of the test to micellization. The highest leakage is observed at the highest OCT quantity. The presented results proved that the leakage on NLM was, quantitatively, greater. Because the incorporation of OCT in the membrane is a fast process, as shown with MD simulations, the initial process of CXF release should be related to the disruption of the membrane by OCT incorporation. Interestingly, the slopes were similar for both the NLM and NegM lipid vesicles, which agrees with results from simulations where the incorporation time was similar.

Statistical analysis of leakage data showed that the results are significantly different. The post hoc test showed that all are significantly different apart from both the NLM and NegM liposomes treated with 0.31 OCT/LIP and 0.25 OCT/LIP and NegM liposomes treated with either 0.25 OCT/LIP or 0.19 OCT/LIP. These results suggest that the disruptive effect is similar in both the NLM and NegM in higher concentrations of OCT. Surprisingly, the release of CXF, especially in lower concentrations of OCT, is quantitatively greater in neutral membranes. This strongly suggests that the disrupting effect of the OCT is not based on electrostatic interactions purely, hence undermining the possibility that the selectivity is based on electrical phenomena. The results are apparently contradictory to leakage experiments reported by Malanovic et al. (13), when PE/PG, PE/PG/CL, and *E. coli* lipid extracts were used as model membranes. For 0.13 OCT/LIP, both PE/PG and PC/PG systems are in agreement (around 10% leakage). Surprisingly, both *E. coli* total lipid extract and pure POPC systems showed 80 and 70% leakage, respectively. The difference occurs at higher (0.31) OCT/LIP, as in the PE/PG system, only 20% leakage is observed but almost 90% leakage in PC/PG systems. However, PE is significantly different lipid then PC when it comes to order parameter, resulting membrane curvature, and ability to assemble into vesicular structures. Moreover, it was reported that the mixing behavior of PC/PG and PE/PG differs. This could be partially caused by different molecular shapes of PE and PC as well as the hydrogen-bonding capacity of PE (62). Such a contrast could result in various lipid packing, different overall physicochemical properties, and different interactions with active molecules such as OCT. These changes could explain the observed differences in leakage induced by OCT between the PC/PG and PE/PG membrane model systems.

To this end, we decided to investigate whether the effect is based on mechanical disruption and selectivity. Firstly, we determined whether the OCT molecule has an effect on mechanical properties of membranes in general. We established bending rigidity changes of OCT incorporation in both the NLM and NegM. Bending rigidity in the NLM system increased after a small (up to 0.1 OCT/LIP) OCT addition. However, it decreased when OCT concentration was around 0.3 OCT/LIP. This was likely caused by membrane integrity loss. There was no statistical significance between 0.3 and 0.5 OCT/LIP. Such an effect was not observed in the case of NegM vesicles, for which the decrease of bending rigidity was observed even in the case of 0.1 OCT/LIP. However, there was no statistical difference between 0.1 and 0.3 OCT/LIP concentration in the NegM, which could correspond to the period of OCT incorporation when negative charges are neutralized by OCT. Only in higher concentrations (0.5 OCT/LIP) was the statistically significant decrease of bending rigidity observed, in much higher concentrations than in the NLM. Given results from leakage and ζ experiments, this could suggest that loss of integrity was observed in higher concentrations in the NegM than in the NLM system. Substantial error bars for bending rigidity measurements could be due to inhomogeneous incorporation to individual GUVs, as well as aggregation in the membrane. The latter is confirmed by simulations. This is particularly visible in the case of 0.1 OCT/LIP. Such a situation would mean that bending rigidity value is a superposition between the vesicles with and without OCT. Bending rigidity change is presented in Fig. 2 *E*. It should be noted that OCT is inducing defects on GUV membranes. It was recently shown (63) that such defects may contribute to slight difference between determined and real membrane bending rigidity. As a result, we considered an alternative mechanism of action of OCT—specifically, that OCT initially influences membrane reorganization (an increase of bending), which is followed by mechanical disruption of the membrane if the OCT concentration is high enough (decrease of bending because of membrane leakage). The lesser leakage observed in the NegM corresponds well with the later decrease of bending compared with the NLM system. This phenomenon could be explained in two ways. Either more OCT concentration is required to neutralize the negative charge of the membrane before the OCT starts disruption or the NegM is much stiffer, hence such an effect. As was shown by Faizi et al., membranes with negatively charged lipids (such as PG) are stiffer (64). Dependence of the ζ potential on the negative surface charge was also investigated, which explains the somewhat paradoxical results obtained from ζ-potential measurements. The increased stiffness of the membrane makes it more resistant to external forces, as similarly seen in the case of stiffening by cholesterol (65). This supports our claim, as it would suggest that negatively charged membranes are much stiffer than neutral ones. Such results could also suggest that a negative charge on the membrane slows down the disruptive effect of OCT. Hence, our observation denies previous literature data explaining the origin of OCT interactions with lipids as a simple electrostatics phenomenon. Additionally, a nondirect premise can be presented, which strengthens this message. *E. coli* cells were reported to change their membrane phenotype to be stiffer to survive the effect of nanomechanical stress caused by ZnO nanorods (66). This suggests that increasing stiffness could be a cell's survival mechanism against mechanical membrane attack. A similar observation is, in a way, presented in our work, in which leakage of the stiffer NegM membrane is inferior to leakage observed in the NLM. To present it in order, the initial effect of OCT, when incorporated into a membrane, induces reorganization that changes its stiffness. For the NLM, if OCT concentration reaches high enough threshold, OCT particles or aggregates start to interact with each, causing a progressive decrease of stiffness, which results in much greater disruption of the membrane and resulted in CXF leakage in our experiment. This is slightly different in the NegM membrane because its native stiffness is higher.

OCT incorporation decreases the stiffness initially, which is followed by a longer period of stability before the disruption of membranes occurs. As shown by the ζ results, aggregation of OCT on the NegM surface is greater; the change is not strong enough to cause the magnitude of the membrane disruption that is observed in the NLM. As a result, quantitatively more OCT particles are required to disrupt the membrane, as additional decrease of the stiffness up to the point of neutral membrane needs to occur and/or negative charge on the membrane requires being balanced. This was observed in the case of 0.25 OCT/LIP and 0.31 OCT/LIP, when the stiffening effect of OCT was similar in both membrane systems (as observed by the fluorescent ratio). On the other hand, a leakage was observed in the OCT concentration region that corresponds to membrane neutralization. Although this can be partially explained by inhomogeneous incorporation of OCT, it also suggests that membrane's mechanical property change is more prevalent than the ζ-potential change.

Summary

In the Introduction, we postulated that the OCT mechanism of action may be based on strong adhesion to charged bacterial components of cell membranes and may be a basis for their selectivity over epithelial cells. Such a mode of action would result in cytoplasm leakage and ultimately cell death. The presented research clearly demonstrates that OCT selectivity nor mechanism is not based on the presence of charged component. Both, leakage was weaker, and incorporation occurred later in the case of charged but stiffer (NegM) membranes. Our results showed that the mechanism of action and likely selectivity of OCT is based on the mechanical property of the membrane, a high-level emerging property appearing after membrane formation and not existing for a single lipid. Even if cell biomechanics in bacteria is poorly investigated, strong differences between mammalian and cells were shown (67). Recently, it was reported that contrary to common conviction, the outer membrane can be stiffer than the cell wall and that mechanical loads are often balanced between these structures (68), which shows that bacteria may be in greater mechanical balance than initially thought. These results are also in agreement with Malanovic et al., who observed that leakage in *E. coli* polar extract was greater than in PE/PG/CL model membrane vesicles (13). It should be noted that those two models differ mostly by acyl-chain length and double bond presence, which strongly modify membrane mechanical properties. Furthermore, mammalian cells are usually stiffer than their lipid membrane models because of the presence of extracellular matrix, which is considered an important mechanical effector (69). The leakage experiment showed that the negatively charged membranes, which are stiffer, are less disruptive in the vicinity of OCT. MD studies showed that depending on membrane composition (and hence mechanics), different aggregate conformations are induced and changes in membrane packing are observed. Combining results from MD and experiments, it could be postulated that the OCT mechanism of action is based on membrane disruption of the membrane.

CHX

Location and behavior

The same procedures as in the case of OCT section were followed in the case of the CHX molecule. Three MD systems were created with a low and high concentrations of CHX for studying the antiseptic agent and lipid membrane interactions and behavior. Snapshots of the initial configuration of systems are presented in Fig. S2.

In the control NLM system, the CHX particle (see Fig. 3 *A*) reached the surface and anchored after 300 ns. In the BacM, the CHX particle reached the surface and anchored much faster, after 167 ns. In the NegM, the CHX particle reached the surface and anchored after 175 ns. In all types of membrane, after incorporation CHX took the shape of a staple, penetrating the monolayer with two acyl chain ends (as shown in Fig. 3 *B*), which is in strong agreement with results presented by Komljenović et al. and van Oosten et al. (70,71). Clearly, the CHX interaction with the membrane was stronger with the BacM, as both reaching the surface and anchoring were faster. However, on the NLM the chlorine atoms from the agent's acyl chain penetrated significantly deepest, reaching the level of 9.1 ± 2.5 Å from the bilayer center. In the case of the BacM and NegM, the CHX reached the levels of 10.3 ± 2.7 and 9.4 ± 3.3 Å, respectively, from the bilayer center. The detailed location of system components such as lipid fragments or agent molecules is presented in the partial density chart in Figs. S5 and S6. There was no significant difference in CHX behavior in 0 mM NaCl BacM and NegM systems besides much faster incorporation to membrane: 35 and 80 ns in the BacM and NegM, respectively. CHX anchored to the membrane and settled down on the edge region of the interphase close to the acyl chains. Interestingly, in the NLM we observed reduced membrane-agent interactions (see Fig. S9). CHX particles diffused above the membrane; the incorporation did not occur. This phenomenon was induced by decreased ion concentration. This suggests that mild ion shielding is required for CHX incorporation to occur when the membrane system is neutral.

In the case of aggregation studies, CHX molecules did not form solid aggregates that would preferentially interact with each other. Particles spread on both leaflets, penetrating them individually and directing their charged chains toward both membranes, leaving the spacer above as presented in Fig. 3 *C*. The entire CHX molecule anchors below the phosphorus hydrophilic groups, on the edge of membrane interphase and a hydrophobic region. Furthermore, CHX behavior was observed approximately for 1 μs, and

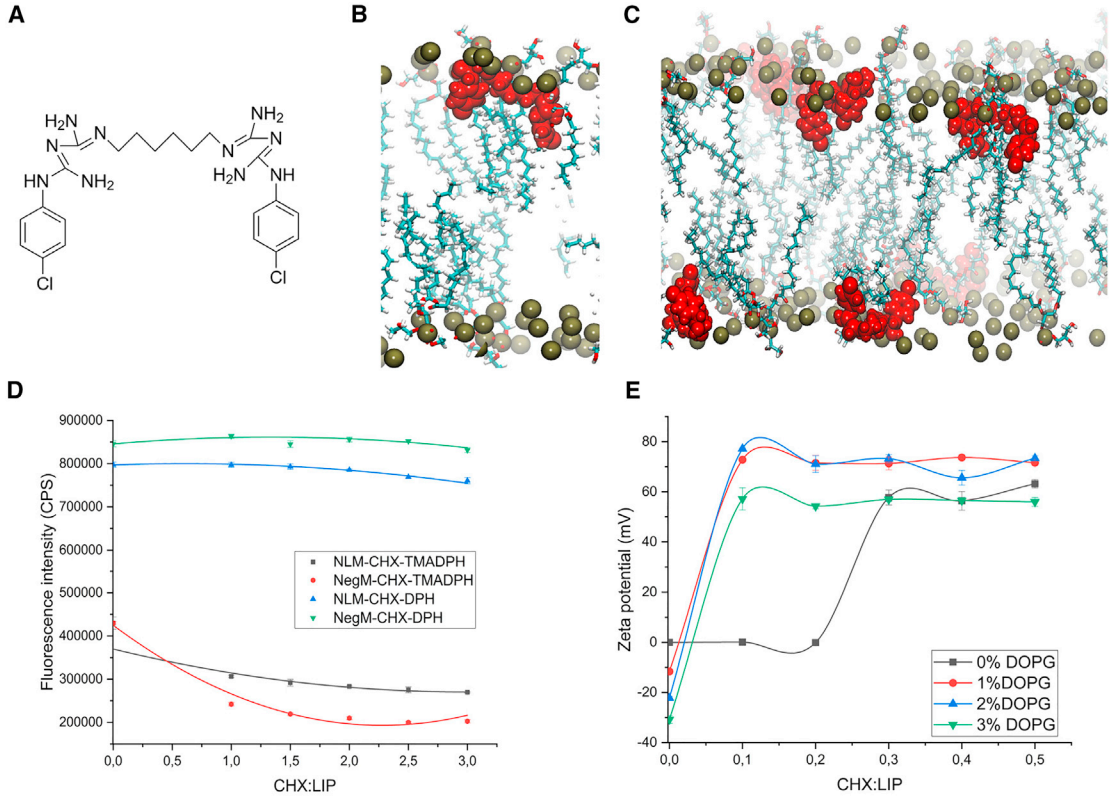

FIGURE 3 (*A*) Chemical structure of CHX and (*B*) single CHX molecule incorporated into BacM (several lipids have been hidden for clarity). OCT molecules, phosphorus atoms from lipid headgroups, and water surface have been colored in red, olive, and blue, respectively. (*C*) Visualization of CHX high concentration system, with agent molecules anchored to NLM, same colors as previously; (*D*) fluorograms from DPH and TMA-DPH probes indicating OCT localization in carbonyl-glycerol region; and (*E*) ζ-potential changes due to CHX titration for the POPC membranes with various DOPG composition. To see this figure in color, go online.

molecules incorporated firmly into the membranes, gently moving around without significantly modifying their positions. We did not see any significant changes in the membrane composition or a destructive effect after CHX action according to MD simulations, which is supported by previous studies (71,72). Furthermore, we did not observe substantial differences in CHX behavior in the 0 mM NaCl BacM and NegM systems. Similarly, CHX did not form aggregates but incorporated separately in a staple form. In the NLM, despite almost 1 μs simulation time, only partial limited CHX-membrane interaction was observed. From seven particles that were present in the system, only six incorporated into the membrane (see Fig. S10). Concerning the lower concentration of CHX in ion membranes, the thickness parameter is greater only in the BacM compared with the pure one, but all types of membranes exposed to CHX showed increased APL (see Table S1), which is in line with van Oosten et al.'s reports, accompanied by little to no change in thickness (71). When analyzing particular lipids, only slight fluctuations of APM are noticed. In no-salt systems, similar behavior is observed. Changes in lateral diffusion were observed after CHX incorporation. Incorporation of a single CHX molecule in general decreases lateral diffusion. Surprisingly, the incorporation of several CHX molecules resulted in an increased lateral diffusion (even when compared to pure systems). More detailed results are presented in Table S3. We cannot conclude with any specific behavior toward either charged and uncharged membranes or specific lipid type. Based on the APL obtained from MD simulation with higher concentrations, it can be directly noted that the parameter increased after CHX incorporation in almost all cases. The APM change reached even 5.3 $Å^2$ in the case of the BacM. Marginal fluctuations are followed in systems with counterions. The evolution of both parameters is included in Tables S1 and S2.

Additionally, DPH and TMA-DPH fluorescence probes were used to assess independently the location of CHX molecules in the membrane. Detailed fluorograms for both probes are presented in Fig. S14. The fluorescence intensity for both probes as a function of CHX concentration is presented in Fig. 3 *D*. Changes in the local environment of the TMA-DPH probe were observed, whereas no major changes were observed in the case of the DPH probe. These results suggest an accumulation of CHX within the outer membrane (interphase area) and no disturbances in the

alkyl-chain area. These results were in agreement with performed MD simulations. CHX did not localize at the level of the hydrophobic layer of the membrane; its preferential accumulation occurred in the edge region of interphase close to the acyl-chain region. This is in line with the previous studies in which, using neutron diffraction, the study CHX hexamethylene was detected near the hydrophobic-hydrophilic interface (70). The changes are not significantly different for NegM liposomes. In both cases, saturation occurs, which may suggest that there is a maximal available space on the surface of the nanocarrier available for CHX. These data are in agreement with the results obtained from the ζ-potential charge measurements.

ζ-potential measurements and partition coefficient

In a similar manner as before, we decided to study membrane structure and stability in the function of CHX concentration by determination of the ζ potential and dynamic light scattering and to evaluate the influence of membrane charge on interaction strength as well. The results presented in Fig. 3 *E* indicate a rapid nature of the interaction between CHX and the NegM compared to the NLM. Specifically, the slope of the ζ-potential change was highest for 1 and 2% DOPG and slightly decreased with 3% DOPG in the membrane. The NegM liposomes were characterized by rapid saturation after the addition of CHX and the determination of the equilibrium state at a level of approximately +60 to +70 mV, which results directly from the partition coefficient of these substances. LogP of CHX was estimated as 5.48 using the SCIGRESS calculation tool. This indicates a high tendency of this substance to be located in the outer part of the membrane. Because the CHX net charge equals zero, experimental determination of water or membrane logP from ζ-potential measurements was not performed. Electrostatic interactions between the CHX molecule and the lipid phosphate groups lead to accumulation of the latter on the surface. The less rapid ζ-potential changes we observe in the NLM, as a peak value of 60 mV was obtained in 0.3 CHX/LIP concentration. The average size of vesicles determined using dynamic light scattering was slightly reduced in increasing CHX concentration (see Fig. S16). We also determined that the ζ-potential changes are not correlated with pH, which remains steady in various agent concentrations (see Fig. S17).

Destructive effect of agent and selectivity

To strengthen our message, we performed membrane self-assembly studies in the presence of CHX (see Fig. 4 *A*). In the case of randomly distributed PC lipids, formation of

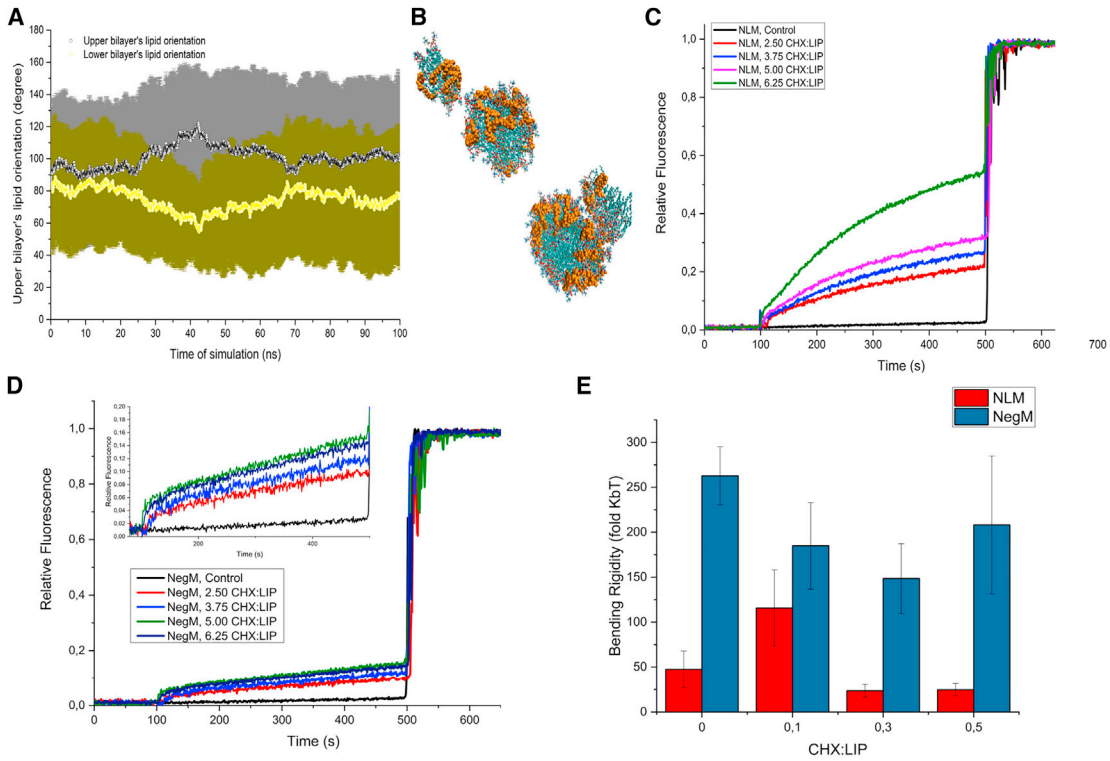

FIGURE 4 (*A*) Self-assembly MD simulation presenting interrupted membrane formation by OCT particles and (*B*) visualization of spherical membrane after self-assembly accompanied by CHX particles. (*C*) CXF leakage from NLM after CHX addition at 100 s, (*D*) CXF leakage from NegM after CHX addition at 100 s, and (*E*) bending rigidity analysis introduced by statistical approach; results obtained from vesicle fluctuation spectroscopy. To see this figure in color, go online.

the bilayer was observed after 60 ns with a 580 kcal/mol increase in VdW energy. However, in the case of randomly distributed lipids with CHX molecules (3:7 CHX/LIP), formation of the bilayer did not occur. Spherical lipid structures covered with CHX were formed instead, which are presented in Fig. 4 *B*. The VdW energy increase equaled 230 kcal/mol. This suggests that CHX influenced the self-assembly process of the membrane. This also indicates that CHX has an impact on membrane structure and/or properties.

To this end, the leakage of CXF loaded inside the liposomes induced by CHX was investigated. With the increasing ratio of CHX/lipid particles, the release of CXF was quantitively greater. However, the doses of CHX used during the experiment were significantly higher than in commercial products or physiological conditions. Interestingly, in the case of the NLM, the leakage of CXF was gradually increasing with time. In the case of the NegM, the leakage was almost linear and hardly noticeable at all. Despite significant doses, in both cases leakage was barely observed. The kinetics for both membranes is presented in Fig. 4, *C* and *D*. Because incorporation of CHX in membrane is a fast process, as we proved in MD simulations, the initial process of CXF release should be rapid, as it would be related to the disruption of the membrane by CHX incorporation. However, because of the quantities used, it is unlikely that the CHX antimicrobial mechanism of action is related to disruption of the membrane fluidity and/or structure. Nevertheless, we assessed the effect of CHX incorporation in the NLM and NegM on bending rigidity value. CHX induced in lower concentrations (0.1 CHX/LIP) an increase in bending rigidity in POPC systems. This was followed by a strong decrease for 0.3 CHX/LIP, making the membrane much more elastic. Successive addition of CHX did not significantly influence membrane mechanical properties. In the case of NegM vesicles, the only significant results were between 0/0.1 CHX/LIP and 0/0.3 CHX/LIP. Both 0.1/0.3 CHX/LIP and 0/0.5 CHX/LIP results were not significant. Such results suggest that after the initial addition of CHX to the NegM system, the additional doses of CHX did not change the mechanical behavior of the membrane. The lack of significance between 0/0.5 CHX/LIP can be easily explained by the presence of membrane defects such as buds that were observed in higher CHX concentrations. Such effects could contribute to measuring higher values of bending rigidity (63). The bending rigidity change is presented in Fig. 4 *E*. Moreover, we employed an average-based approach for bending rigidity determination presented in Fig. S19. It should be noted that CHX induces an ellipsoidal shape on GUV membranes. It was recently shown (63) that this could contribute to a slight difference between determined and real membrane bending rigidity. Interestingly, although the decrease of bending rigidity was substantial in the case of the NLM, mechanical disruption of the membrane did not occur, as clearly seen in leakage experiments. The change of bending rigidity was much lower in the case of the NegM system, which corresponds well with the results from leakage experiments, in which stronger leakage was observed in the NLM system. Nevertheless, the observed leakage and changes in bending rigidity are not magnitude enough to assume that CHX is inducing the integrity loss based on mechanical properties. Neither the results of any experiments nor those of simulations indicated that there is any kind of electrostatic selectivity.

Summary

It was suggested by Epand et al. (43) that the possible antimicrobial mechanism of membrane-targeting agents is related to the disruption of membrane ability to spontaneously form microdomains. For instance, in *E. coli*, cardiolipin domains were observed under the microscope (73). With a significant change of mechanical properties, lack of vesicle leakage, and nonspecific changes in APL and lateral diffusion, we assume that the antimicrobial effect of CHX is related to changes in stiffness of the membrane, which can result in disruption of microdomain formation and/or loss of proteostasis for transmembrane proteins, which are crucial for microbe survival (74). All investigated systems were homogeneous (no domains); hence, possible effects due to heterogeneity could not be observed.

CONCLUSIONS

In this study, we have made an attempt to unravel the mechanism and selectivity of antimicrobial candidates, octenidine and chlorhexidine, in various lipid membrane systems. In molecular dynamics studies, we selected three types of lipid composition to represent neutral, negatively charged, and bacterial membranes. Our results indicate that a single molecule of both OCT and CHX is incorporated into all membranes in the same staple shape. A difference was observed with increasing concentration of compounds. In reference to OCT, an aggregate was formed first, and interaction with membrane was noted afterward. We also observed several shapes of aggregates depending on the lipid composition. The opposite tendency occurred in CHX behavior. It penetrated the bilayers singly and did not form aggregates, which is caused by the noticeably smaller partition coefficient, logP. Moreover, we assume that OCT forms aggregates preferentially to minimize the entropy of the system. Observed results of APL, membrane thickness, and lateral diffusion values indicated that both compounds firmly interact with all types of membranes. We determined by TMA-DPH and DPH fluorescent probes that accumulation of the OCT and CHX molecules is located in the carbonyl-glycerol region, which is in agreement with our simulations. To observe preferential accumulation and the particles' influence on membrane surface charge, we performed ζ-potential measurements. Interestingly,

interactions with the NLM were more rapid compared with the NegM one based on ζ-potential kinetics. We suppose that mutual repulsion of these compounds and their partition coefficients saturate the surface charge and neutralize the negative membrane charges; hence, the ζ-potential kinetics for NegM are slower for OCT and CHX. The ζ potential emphasized the differences in interaction between CHX and OCT with the NegM, despite the comparable localization in membrane. To detect the destructive properties of both molecules, we investigated self-assembly ability in MD of lipids in the presence of antimicrobial agents and CXF leakage from liposomes as an effect of agent presence. In both cases, membrane self-assembly was affected. Spherical structures were formed instead of a pure bilayer. The damaging properties of molecules are also noticeable during CXF leakage. However, they were less distinctive in the case of CHX. The NLM's exposure to OCT and CHX caused more intensive leakage compared with the NegM. We also investigated the effect of the investigated substances on membrane mechanical properties. The bending coefficient decreased significantly in both cases, making the membrane much more elastic. The presented research indicates that OCT shows a selective effect over membrane mechanical properties. Bending and stiffness of membrane occurs as an emerging property that could possibly serve as a means of selectivity. By further inducing mechanical changes, OCT would induce mechanical defects and loss of membrane integrity. Such a mode of action would result in cytoplasm leakage and ultimately cell death. Taking into account the change in mechanical properties, the effect of membrane self-aggregation, and nonspecific changes in both APL and lateral diffusion, we assume that the antimicrobial effect of CHX is related to decreased stiffness of the membrane, which can result in the disruption of microdomain formation and/or loss of proteostasis. In the case of CHX, mechanical changes did not induce considerable leakage of CXF from the liposomes. As a result, we believe that the possible CHX antimicrobial mechanism of membrane-targeting agents is based on the impediment of the membrane's ability to spontaneously form microdomains.

SUPPORTING MATERIAL

Supporting material can be found online at https://doi.org/10.1016/j.bpj.2021.06.027.

AUTHOR CONTRIBUTIONS

S.K., D.D., and K.S.-P. designed the research. D.D., M.R., K.S.-P., and B.H.-L. performed the experiments. M.R. and D.D. performed the MD simulations. M.R., D.D., and K.S.-P. analyzed data. S.K. provided funding and materials. M.R. and D.D. wrote the manuscript, which was revised by all authors.

ACKNOWLEDGMENTS

The authors gratefully acknowledge helpful discussions and computational resources with Mounir Tarek.

This work was possible thanks to financial support from National Science Centre (grant number 2015/19/B/NZ7/02380).

REFERENCES

1. Russell, A. D. 2002. Antibiotic and biocide resistance in bacteria: introduction. *J. Appl. Microbiol.* 92 (*Suppl*):1S–3S.
2. World Health Organization. 2014. Antimicrobial resistance: global report on surveillance. WHO Press, Switzerland https://apps.who.int/iris/handle/10665/112642.
3. Ventola, C. L. 2015. The antibiotic resistance crisis: part 1: causes and threats. *P T.* 40:277–283.
4. Kong, K. F., L. Schneper, and K. Mathee. 2010. Beta-lactam antibiotics: from antibiosis to resistance and bacteriology. *APMIS.* 118:1–36.
5. Kramer, A. 2000. Hand disinfection and antiseptic of skin, mucous membranes, and wounds. *In* Dermatopharmacology of Topical Preparations. B. Gabard, C. Surber, P. Elsner, and P. Treffel, eds. Springer, pp. 121–134.
6. Gilbert, P., and L. E. Moore. 2005. Cationic antiseptics: diversity of action under a common epithet. *J. Appl. Microbiol.* 99:703–715.
7. Assadian, O. 2016. Octenidine dihydrochloride: chemical characteristics and antimicrobial properties. *J. Wound Care.* 25 (*Suppl 3*):S3–S6.
8. Sedlock, D. M., and D. M. Bailey. 1985. Microbicidal activity of octenidine hydrochloride, a new alkanediylbis[pyridine] germicidal agent. *Antimicrob. Agents Chemother.* 28:786–790.
9. Freeman, D. E., and J. A. Auer. 2012. Instrument preparation, sterilization, and antiseptics. *In* Equine Surgery. J. A. Auer and J. A. Stick, eds. Elsevier Inc., pp. 98–111.
10. Schneider, L. A., A. Körber, …, J. Dissemond. 2007. Influence of pH on wound-healing: a new perspective for wound-therapy? *Arch. Dermatol. Res.* 298:413–420, Published online November 8, 2006.
11. Al-Doori, Z., P. Goroncy-Bermes, …, D. Morrison. 2007. Low-level exposure of MRSA to octenidine dihydrochloride does not select for resistance. *J. Antimicrob. Chemother.* 59:1280–1281.
12. Kodedová, M., K. Sigler, …, D. Gášková. 2011. Fluorescence method for determining the mechanism and speed of action of surface-active drugs on yeast cells. *Biotechniques.* 50:58–63.
13. Malanovic, N., A. Ön, …, K. Lohner. 2020. Octenidine: novel insights into the detailed killing mechanism of Gram-negative bacteria at a cellular and molecular level. *Int. J. Antimicrob. Agents.* 56:106146.
14. Hübner, N.-O., J. Siebert, and A. Kramer. 2010. Octenidine dihydrochloride, a modern antiseptic for skin, mucous membranes and wounds. *Skin Pharmacol. Physiol.* 23:244–258.
15. Brill, F., P. Goroncy-Bermes, and W. Sand. 2006. Influence of growth media on the sensitivity of *Staphylococcus aureus* and *Pseudomonas aeruginosa* to cationic biocides. *Int. J. Hyg. Environ. Health.* 209:89–95.
16. Szostak, K., A. Czogalla, …, M. Langner. 2018. New lipid formulation of octenidine dihydrochloride. *J. Liposome Res.* 28:106–111.
17. Nicolae Dopcea, G., I. Dopcea, …, F. Matei. 2020. Resistance and cross-resistance in *Staphylococcus spp.* strains following prolonged exposure to different antiseptics. *J. Glob. Antimicrob. Resist.* 21:399–404.
18. Shepherd, M. J., G. Moore, …, L. J. Bock. 2018. *Pseudomonas aeruginosa* adapts to octenidine in the laboratory and a simulated clinical setting, leading to increased tolerance to chlorhexidine and other biocides. *J. Hosp. Infect.* 100:e23–e29.
19. Horner, C., D. Mawer, and M. Wilcox. 2012. Reduced susceptibility to chlorhexidine in staphylococci: is it increasing and does it matter? *J. Antimicrob. Chemother.* 67:2547–2559.

20. Kanisavaran, Z. M. 2008. Chlorhexidine gluconate in endodontics: an update review. *Int. Dent. J.* 58:247–257.

21. Eggers, M., T. Koburger-Janssen, …, S. Müller. 2018. Bactericidal and virucidal activity of povidone-iodine and chlorhexidine gluconate cleansers in an in vivo hand hygiene clinical simulation study. *Infect. Dis. Ther.* 7:235–247.

22. do Amorim, C. V. G., C. E. Aun, and M. P. A. Mayer. 2004. Susceptibility of some oral microorganisms to chlorhexidine and paramonochlorophenol. *Braz. Oral Res.* 18:242–246.

23. Kropinski, A. M., J. Kuzio, …, R. E. W. Hancock. 1982. Chemical and chromatographic analysis of lipopolysaccharide from an antibiotic-supersusceptible mutant of *Pseudomonas aeruginosa*. *Antimicrob. Agents Chemother.* 21:310–319.

24. Thomas, B., and D. J. Stickler. 1979. Chlorhexidine resistance and the lipids of Providencia stuartii. *Microbios.* 24:141–150.

25. Wright, N. E., and P. Gilbert. 1987. Influence of specific growth rate and nutrient limitation upon the sensitivity of *Escherichia coli* towards chlorhexidine diacetate. *J. Appl. Bacteriol.* 62:309–314.

26. Copin, R., W. E. Sause, …, B. Shopsin. 2019. Sequential evolution of virulence and resistance during clonal spread of community-acquired methicillin-resistant *Staphylococcus aureus*. *Proc. Natl. Acad. Sci. USA.* 116:1745–1754.

27. Cieplik, F., N. S. Jakubovics, …, A. Al-Ahmad. 2019. Resistance toward chlorhexidine in oral bacteria-is there cause for concern? *Front. Microbiol.* 10:587.

28. Cheung, H. Y., M. M. K. Wong, …, S. K. Chiu. 2012. Differential actions of chlorhexidine on the cell wall of *Bacillus subtilis* and *Escherichia coli*. *PLoS One.* 7:e36659.

29. Chawner, J. A., and P. Gilbert. 1989. Interaction of the bisbiguanides chlorhexidine and alexidine with phospholipid vesicles: evidence for separate modes of action. *J. Appl. Bacteriol.* 66:253–258.

30. Chawner, J. A., and P. Gilbert. 1989. Adsorption of alexidine and chlorhexidine to *Escherichia coli* and membrane components. *Int. J. Pharm.* 55:209–215.

31. Davies, A. 1973. The mode of action of chlorhexidine. *J. Periodontal Res. Suppl.* 12:68–75.

32. Hugo, W. B., and A. R. Longworth. 1965. Cytological aspects of the mode of action of chlorhexidine diacetate. *J. Pharm. Pharmacol.* 17:28–32.

33. Elferink, J. G. R., and H. L. Booij. 1974. Interaction of chlorhexidine with yeast cells. *Biochem. Pharmacol.* 23:1413–1419.

34. Hugo, W. B., and A. R. Longworth. 1964. Some aspects of the mode of action of chlorhexidine. *J. Pharm. Pharmacol.* 16:655–662.

35. Rye, R. M., and D. Wiseman. 1968. Some observations on the use of absorbance measurements in bacteriology. *J. Pharm. Pharmacol.* 20:23S–25S.

36. Chawner, J. A., and P. Gilbert. 1989. A comparative study of the bactericidal and growth inhibitory activities of the bisbiguanides alexidine and chlorhexidine. *J. Appl. Bacteriol.* 66:243–252.

37. Longworth, A. R. 1971. Inhibition and Destruction of the Microbial Cell. Academic Press, New York.

38. Banerjee, D., U. Sarkar, and D. Roy. 2013. Multicomponent adsorption of chlorhexidine gluconate in presence of a cationic surfactant: role of electrostatic interactions and surface complexation. *J. Environ. Chem. Eng.* 1:241–251.

39. Freitas, L. B., N. Vassilakos, and T. Arnebrant. 1993. Interactions of chlorhexidine with salivary films adsorbed at solid/liquid and air/liquid interfaces. *J. Periodontal Res.* 28:92–97.

40. Costalonga, B. L. P., R. C. da Silva, …, C. Molina. 2012. Interaction of chlorhexidine with biomembrane models on glass ionomer by using the Langmuir-Blodgett technique. *Colloids Surf. B Biointerfaces.* 97:57–61.

41. Gottenbos, B., D. W. Grijpma, …, H. J. Busscher. 2001. Antimicrobial effects of positively charged surfaces on adhering Gram-positive and Gram-negative bacteria. *J. Antimicrob. Chemother.* 48:7–13.

42. Sohlenkamp, C., and O. Geiger. 2016. Bacterial membrane lipids: diversity in structures and pathways. *FEMS Microbiol. Rev.* 40:133–159.

43. Epand, R. M., and R. F. Epand. 2009. Lipid domains in bacterial membranes and the action of antimicrobial agents. *Biochim. Biophys. Acta.* 1788:289–294.

44. Drabik, D., J. Doskocz, and M. Przybyło. 2018. Effects of electroformation protocol parameters on quality of homogeneous GUV populations. *Chem. Phys. Lipids.* 212:88–95.

45. Drabik, D., M. Przybyło, …, M. Langner. 2016. The modified fluorescence based vesicle fluctuation spectroscopy technique for determination of lipid bilayer bending properties. *Biochim. Biophys. Acta.* 1858:244–252.

46. Freire, J. M., M. M. Domingues, …, M. A. R. B. Castanho. 2011. Using zeta-potential measurements to quantify peptide partition to lipid membranes. *Eur. Biophys. J.* 40:481–487.

47. Frisch, M. J., G. W. Trucks, X. Li…, 2016. Gaussian 16, Revision. Gaussian Inc., Wallingford CT https://gaussian.com/gaussian16/.

48. Jo, S., T. Kim, …, W. Im. 2008. CHARMM-GUI: a web-based graphical user interface for CHARMM. *J. Comput. Chem.* 29:1859–1865.

49. Humphrey, W., A. Dalke, and K. Schulten. 1996. VMD: visual molecular dynamics. *J. Mol. Graph.* 14:33–38, 27–28..

50. Giorgino, T. 2019. Computing diffusion coefficients in macromolecular simulations: the diffusion coefficient tool for VMD. *J. Open Source Software.* 4:1698.

51. Kholina, E. G., I. B. Kovalenko, …, P. S. Orekhov. 2020. Cationic antiseptics facilitate pore formation in model bacterial membranes. *J. Phys. Chem. B.* 124:8593–8600.

52. Lentz, B. R. 1989. Membrane "fluidity" as detected by diphenylhexatriene probes. *Chem. Phys. Lipids.* 50:171–190.

53. Demchenko, A. P., Y. Mély, …, A. S. Klymchenko. 2009. Monitoring biophysical properties of lipid membranes by environment-sensitive fluorescent probes. *Biophys. J.* 96:3461–3470.

54. do Canto, A. M. T. M., J. R. Robalo, …, L. M. S. Loura. 2016. Diphenylhexatriene membrane probes DPH and TMA-DPH: a comparative molecular dynamics simulation study. *Biochim. Biophys. Acta.* 1858:2647–2661.

55. Cundall, R. B., I. Johnson, …, I. H. Munro. 1979. Photophysical properties of DPH derivatives. *Chem. Phys. Lett.* 64:39–42.

56. Prendergast, F. G., R. P. Haugland, and P. J. Callahan. 1981. 1-[4-(Trimethylamino)phenyl]-6-phenylhexa-1,3,5-triene: synthesis, fluorescence properties, and use as a fluorescence probe of lipid bilayers. *Biochemistry.* 20:7333–7338.

57. Poojari, C., N. Wilkosz, …, T. Róg. 2019. Behavior of the DPH fluorescence probe in membranes perturbed by drugs. *Chem. Phys. Lipids.* 223:104784.

58. Nazari, M., M. Kurdi, and H. Heerklotz. 2012. Classifying surfactants with respect to their effect on lipid membrane order. *Biophys. J.* 102:498–506.

59. Stewart, C. A., Y. Finer, and B. D. Hatton. 2018. Drug self-assembly for synthesis of highly-loaded antimicrobial drug-silica particles. *Sci. Rep.* 8:895.

60. Pan, H., J. N. Marsh, …, S. A. Wickline. 2012. Postformulation peptide drug loading of nanostructures. Methods in Enzymology. Academic Press Inc, pp. 17–39.

61. Chen, R. F., and J. R. Knutson. 1988. Mechanism of fluorescence concentration quenching of carboxyfluorescein in liposomes: energy transfer to nonfluorescent dimers. *Anal. Biochem.* 172:61–77.

62. Sevcsik, E., G. Pabst, …, K. Lohner. 2008. Interaction of LL-37 with model membrane systems of different complexity: influence of the lipid matrix. *Biophys. J.* 94:4688–4699.

63. Faizi, H. A., C. J. Reeves, …, R. Dimova. 2020. Fluctuation spectroscopy of giant unilamellar vesicles using confocal and phase contrast microscopy. *Soft Matter.* 16:8996–9001.

64. Faizi, H. A., S. L. Frey, …, P. M. Vlahovska. 2019. Bending rigidity of charged lipid bilayer membranes. *Soft Matter.* 15:6006–6013.

65. Drabik, D., M. Gavutis, …, A. R. Ulčinas. 2020. Determination of the mechanical properties of model lipid bilayers using atomic force microscopy indentation. *Langmuir.* 36:13251–13262.

66. Matuła, K., Ł. Richter, …, R. Hołyst. 2019. Phenotypic plasticity of *Escherichia coli* upon exposure to physical stress induced by ZnO nanorods. *Sci. Rep.* 9:8575.

67. Harper, C. E., and C. J. Hernandez. 2020. Cell biomechanics and mechanobiology in bacteria: challenges and opportunities. *APL Bioeng.* 4:021501.

68. Rojas, E. R., G. Billings, …, K. C. Huang. 2018. The outer membrane is an essential load-bearing element in Gram-negative bacteria. *Nature.* 559:617–621.

69. Handorf, A. M., Y. Zhou, …, W. J. Li. 2015. Tissue stiffness dictates development, homeostasis, and disease progression. *Organogenesis.* 11:1–15.

70. Komljenović, I., D. Marquardt, …, E. Sternin. 2010. Location of chlorhexidine in DMPC model membranes: a neutron diffraction study. *Chem. Phys. Lipids.* 163:480–487.

71. Van Oosten, B., D. Marquardt, …, T. A. Harroun. 2014. Small molecule interaction with lipid bilayers: a molecular dynamics study of chlorhexidine. *J. Mol. Graph. Model.* 48:96–104.

72. Van Oosten, B., D. Marquardt, and T. A. Harroun. 2017. Testing high concentrations of membrane active antibiotic chlorhexidine via computational titration and calorimetry. *J. Phys. Chem. B.* 121:4657–4668.

73. Fishov, I., and C. L. Woldringh. 1999. Visualization of membrane domains in *Escherichia coli*. *Mol. Microbiol.* 32:1166–1172.

74. Barák, I., and K. Muchová. 2013. The role of lipid domains in bacterial cell processes. *Int. J. Mol. Sci.* 14:4050–4065.